genes

MDPI

Article

Uncovering Porphyrin Accumulation in the Tumor Microenvironment

Swamy R. Adapa [1,2], Abdus Sami [3], Pravin Meshram [2], Gloria C. Ferreira [3,4] and Rays H. Y. Jiang [1,2,*]

[1] USF Genomics Program, Center for Global Health and Infectious Diseases, College of Public Health, University of South Florida, Tampa, FL 33612, USA; swamyrakesh@usf.edu
[2] Global and Planetary Health, College of Public Health, University of South Florida, Tampa, FL 33612, USA; pdmeshram@usf.edu
[3] Department of Molecular Medicine, Morsani College of Medicine, University of South Florida, Tampa, FL 33612, USA; abdussami@usf.edu (A.S.); gferreir@usf.edu (G.C.F.)
[4] Department of Chemistry, College of Arts and Sciences, University of South Florida, Tampa, FL 33620, USA
* Correspondence: jiang2@usf.edu; Tel.: +1-813-974-4541

Abstract: Heme, an iron-containing tetrapyrrole, is essential in almost all organisms. Heme biosynthesis needs to be precisely regulated particularly given the potential cytotoxicity of protoporphyrin IX, the intermediate preceding heme formation. Here, we report on the porphyrin intermediate accumulation within the tumor microenvironment (TME), which we propose to result from dysregulation of heme biosynthesis concomitant with an enhanced cancer survival dependence on mid-step genes, a process we recently termed "*Porphyrin Overdrive*". Specifically, porphyrins build up in both lung cancer cells and stromal cells in the TME. Within the TME's stromal cells, evidence supports cancer-associated fibroblasts (CAFs) actively producing porphyrins through an imbalanced pathway. Conversely, normal tissues exhibit no porphyrin accumulation, and CAFs deprived of tumor cease porphyrin overproduction, indicating that both cancer and tumor-stromal porphyrin overproduction is confined to the cancer-specific tissue niche. The clinical relevance of our findings is implied by establishing a correlation between imbalanced porphyrin production and overall poorer survival in more aggressive cancers. These findings illuminate the anomalous porphyrin dynamics specifically within the tumor microenvironment, suggesting a potential target for therapeutic intervention.

Keywords: heme; porphyrin; protoporphyrin IX; tumor microenvironment; cancer-associated fibroblasts

Citation: Adapa, S.R.; Sami, A.; Meshram, P.; Ferreira, G.C.; Jiang, R.H.Y. Uncovering Porphyrin Accumulation in the Tumor Microenvironment. *Genes* **2024**, *15*, 961. https://doi.org/10.3390/genes15070961

Academic Editor: Christos K. Kontos

Received: 13 May 2024
Revised: 9 July 2024
Accepted: 10 July 2024
Published: 22 July 2024

1. Introduction

Cancer, as a complex and multifaceted spectrum of diseases, remains a significant challenge in medical research and for treatment [1]. The interplay between cancer cells and their microenvironment has revealed novel pathways for understanding and addressing the relentless adversary that is cancer. The molecular landscape of the tumor microenvironment (TME) is diverse and has intricate molecular mechanisms [2,3]. The emergence of dysregulated metabolism in the TME stands out as a compelling entity with both diagnostic and therapeutic potential [4,5].

Cancer cells and components of the TME maintain dynamic and mutual interactions to sustain cancer cell survival and proliferation; the tumor cells exhibit distinctive metabolic alterations that contribute to the hallmarks of malignancy [6]. Namely, the Warburg effect, characterized by increased aerobic glycolysis, is a prevalent metabolic shift in which cancer cells favor glycolysis over oxidative phosphorylation even in the presence of oxygen [7,8]. The heightened dependence on glutamine metabolism supports rapid proliferation, providing essential precursors for biosynthetic pathways and sustaining the tricarboxylic acid (TCA) cycle [9]. Dysregulated lipid metabolism causes increased fatty acid synthesis to fulfill the demands for membrane biogenesis and energy production [10,11]. One-carbon

(1C) metabolism, involving folate-mediated 1C-unit transfers in serine-glycine and methionine syntheses, adjusts to respond to the higher demands for nucleotide synthesis and epigenetic maintenance [12–14]. Redox homeostasis disruption, with elevated reactive oxygen species (ROS) levels, contributes to genomic instability and cancer progression [15]. Furthermore, shifts in amino acid metabolism, such as increased consumption of serine and glycine [14], play pivotal roles in sustaining protein synthesis and other cellular processes.

Porphyrins are cyclic tetrapyrroles with highly conjugated aromatic macrocycles [16]. Because of these π-conjugated structures, porphyrins and porphyrin derivatives exhibit characteristic electronic features, and photophysical and electrochemical properties [17–19], which clearly contribute to their many different biological roles [20]. For example, porphyrin derivatives form chromophoric assemblies involved in light-harvesting for photosynthesis. Metalated porphyrins, typically resulting from chelation of a specific divalent metal ion into the porphyrin macrocyle, have an even larger plethora of functions since the chelated metal ion can bestow redox activity and an additional ligand coordination site. Ferrous iron (Fe^{2+})-bound protoporphyrin IX (PPIX) or heme b (hereon referred to as heme) stands out as a metalated porphyrin with biochemical and physiological activities that go beyond oxygen transport, oxygen storage, electron transfer, and catalysis [20]. Heme-bound proteins act as heme-responsive sensors and regulate transcription [20–24], microRNA splicing and processing [25], translation [26], heme degradation [27], protein degradation [28,29], K^+ channel function [30], redox status [30–32], and protein–protein interactions [20]. The enzyme-catalyzed chelation of Fe^{2+} in PPIX corresponds to the terminal step of the heme biosynthetic pathway [33–35]. This reaction is finely regulated as both PPIX and iron ion are potentially cytotoxic [36,37]. However, and in a somewhat ironic twist, the uncontrolled production and accumulation of PPIX, typically observed in cancer, can serve as both a diagnostic marker and a therapeutic agent [38]. We recently coined the term "Porphyrin Overdrive" to describe this process [38]. The fluorescence emission properties of porphyrins like PPIX enable non-invasive tumor imaging and cancer detection [39]. Because porphyrins are photosensitizers, they are employed in photodynamic therapy (PDT) [40]. Light activation of the porphyrins accumulated in cancer cells leads to ROS generation and their selectively targeted cell death [40].

The TME is a dynamic and heterogeneous milieu of cells where the tumor resides. It comprises normal cells, including immune and stromal cells, signaling molecules, extracellular matrix, and blood vessels that enclose and feed the tumor cells [3]. Recent investigations have unveiled that dysregulation of heme biosynthesis within the TME supports cancer [41,42]. In fact, metabolic patterns for heme production and transport are altered in comparison to those in normal cells [41–44]. In this study, we delineate a novel facet of metabolic rewiring in the TME. We demonstrate that porphyrin production occurs in both cancer cells and stromal cells in the TME. Porphyrins (i.e., heme intermediates) play a prominent role as their biosynthesis, and not that of heme per se, is linked to cancer aggressiveness. Significantly, porphyrin production not only sustains cancer cell survival and proliferation, but also influences clinical outcomes. Thus, understanding the dynamics of porphyrin production in the TME holds the promise of unveiling novel insights into the metabolic adaptations that sustain tumorigenesis.

2. Materials and Methods

2.1. Cell Culture, Growth, and Quantification

The lung cancer cell line H460 was kindly provided by Gina DeNicola lab at Moffitt Cancer Institute, FL. USA. The onco-transformed BJ fibroblasts were kindly provided by Robert A. Weinberg Lab at MIT, MA, USA. Cell culture, proliferation, and quantification procedures were carried out utilizing human lung cancer cell lines. Cells were cultivated in RPMI 1640 medium (Gibco, Waltham, MA USA), supplemented with 10% fetal bovine serum (Sigma, St. Louis, MO, USA), 2 mM L-glutamine, and additional components such as gentamicin (1000×, Fisher, Plano, TX, USA, Cat No. 15-710-072) and PennStrepNeo solution (100×, Fisher, Plano, TX, USA, Cat No. 15640-055). The incubation of cells occurred

at 37 °C in a humidified 5% CO_2 atmosphere to facilitate optimal growth conditions. The stock solutions of 5-aminolevulinic acid hydrochloride (ALA) and glycine were prepared by dissolving them in distilled water and phenol red-free culture medium, respectively. ALA, sourced from Alfa Aesar (Cat No. A16942ME), was stored at −20 °C with a stock concentration of 1.0 M. Glycine, acquired from Fisher Chemical (Cat No. BP381-500), was stored as a 1 M stock solution. Cancer cells were initially plated at a density of 1–2 × 10^5/mL, and cell counting, performed using trypan blue exclusion (Corning, New York, NY, USA, Cat No. 25-900-CI), was carried out over time. As part of the quantification process, total cell numbers were determined based on the passage dilution at each time point.

2.2. Heme Biosynthetic Pathway-Related Gene Expression Analysis

Analysis of the gene expression patterns for the enzymes of the heme biosynthetic pathway in tumors and normal tissues was performed using the Genotype-Tissue Expression (GTEx) project [45,46] and The Cancer Genome Atlas (TCGA) program [47] as data resources. The heme biosynthetic pathway gene expression patterns in tumors vs. matched normal tissues were used for analysis. Briefly, this analysis involved a thorough comparison of gene expression profiles for enzymes involved in the heme biosynthetic pathway between tumor samples and their corresponding paired normal tissues. Non-parametric pairwise Wilcoxon comparisons were conducted between normal and tumor samples. The expression levels of each gene involved in heme biosynthesis in both normal and tumor tissues were examined, and specific changes associated with each biosynthetic step in the linear pathway were analyzed to infer significant expression differences between tumor and normal tissues.

2.3. Heme CRISPR Cancer Gene Essentiality Analysis

The essentiality analysis of cancer genes using CRISPR/Cas9 was conducted utilizing data sourced from the DepMap Portal, following established methodologies [48–50]. Whole-genome CRISPR/Cas9 datasets were employed to identify significantly depleted growth of mutant cells resulting from specific gene knockouts in pooled experiments. Gene essentiality was inferred from the dependency of a given gene, deduced from CRISPR/Cas9 gRNA-mediated gene knockout. Essential scores were utilized to assess cell growth fitness, with lower scores indicating a greater impact on cell viability upon gene loss. Specifically, scores of 0, <0, and >0 denoted no fitness change, fitness loss, and fitness gain (implying potential growth advantage for the cell line) under the assay conditions. To address copy number bias in whole-genome CRISPR/Cas screens, the method outlined in [48,49] was applied, involving the computation of the mean of sgRNAs versus the control plasmid library.

Identification of commonly essential genes was based on their significance for the fitness of most cell lines across various cancer types [51,52]. For the analysis of in vivo gene essentiality in pancreatic and lung cancer models, data published in [53] were used to specifically investigate genes related to the heme biosynthetic pathway enzymes and heme transporters.

2.4. In Vitro Primary Human Cell Culture, Quantification, and Imaging

Plates having 384 wells (Greiner Bio-One, Kremsmünster, Austria, Cat No. 781091) were aseptically handled in a class II biosafety cabinet and then placed in a secondary container, serving as a lid to control evaporation (i.e., plates were positioned in large assay pans). Immediately before seeding, wells were filled with 20 µL advanced DMEM/F12 plating medium (Gibco, Waltham, MA, USA, Cat No. 12634010) supplemented with, 10% FBS (Hyclone, Logan, UT, USA, Cat No. SH30070), 2 mM L-Glutamine (Invitrogen, Carlsbad, CA, USA, Cat No. 25030-081), 10 µM Y-27632 dihydrochloride (Tocris Bioscience, Bristol, UK, Cat No. 1254), 1× Pen-Strep-Neo solution (100×, Fisher, Waltham, MA, USA, Cat No. 15640-055) and 20 µM gentamicin (1000×, Fisher, Waltham, MA, USA, Cat No. 15-710-072). Cryopreserved primary human cells (BioIVT, Westbury, NY, USA) were thawed by immersion in a 37 °C water bath for 2 min, sterilized with 70% ethanol in a sterile

field, and their contents were directly added to 4 mL of plate medium. Live and dead cells were quantified through trypan blue exclusion on a Neubauer improved hemocytometer. The cell density was adjusted to 1×10^3 live cells μL^{-1}, and 18 µL of cell suspension was added to each well. Medium exchanges with the plating medium, as described earlier, were performed thrice weekly. The cells were incubated with 1.0 mM ALA at 37 °C for 4 h, and both ALA-treated and non-treated cells were handled under very-low-light conditions. During the last 45 min of incubation, a staining solution, diluted in phenol-free, serum-free RPMI (Gibco, Waltham, MA, USA, Cat No. 11835055), and containing Hoechst 33342 (Life Technologies, Carlsbad, CA, USA, Cat No. H3570) at a final concentration of 10 µM, was added to the cells. Live cell imaging was conducted on a CellInsight CX7 High-Content Screening Platform (Thermo Fisher Scientific, Waltham, MA, USA), with each well counted for cell nuclei staining.

2.5. In Vitro Cancer Cell Line Culture, Quantification, and Imaging

Cells were allowed to grow until reaching 70%. In the in vitro culture of cancer cell lines, cryopreserved cells were thawed, suspended in a pre-prepared culture medium, and then transferred to a collagen-coated T75 flask (Corning, New York, NY, USA, Cat No. 354236) at a density of 5 $\mu g/cm^2$. The culture medium was composed of a 1:1 (v/v) mixture of F12 base medium (Invitrogen, Carlsbad, CA, USA, Cat No. 11765-054) and MEM base medium (Invitrogen, Carlsbad, CA, USA, Cat No. A10490-01), supplemented with 10% FBS (Hyclone, Logan, UT, USA, Cat No. SH30070), 1.0 M HEPES (Invitrogen, Carlsbad, CA, USA, Cat No. 15630-080), and 200 mM glutamine (Invitrogen, Carlsbad, CA, USA, Cat No. 25030-081) [54]. Cells were allowed to grow until reaching 70% confluence, with medium changes every other day. Upon reaching the desired confluence, cells were trypsinized using TrypLE™ Express Enzyme (1×) (Gibco, Waltham, MA, USA, Cat No. 12605028), washed with culture medium, and then seeded at a density of 6000 cells/well in 384-well plates (Greiner Bio-One, Kremsmünster, Austria, Cat No. 781091). The cells were cultured in 20 µL of the above medium per well and incubated at 37 °C either in the absence or presence of 1.0 mM ALA for 4 h. Both ALA-treated and non-treated cells were handled under very-low-light conditions.

During the final 45 min of incubation, a staining solution, diluted in phenol-free, serum-free RPMI (Gibco, Waltham, MA, USA, Cat No. 11835055) and containing Hoechst 33342 (Life Technologies, Carlsbad, CA, USA, Cat No. H3570) at a final concentration of 10 µM, was added to the cells. Live cell imaging was conducted using a CellInsight CX7 High-Content Screening Platform (Thermo Fisher Scientific, Waltham, MA, USA), with each well of the 384-well plate capturing images from 15 fields at 20× magnification for nuclei staining.

2.6. Cellular PPIX Quantification

Quantification of intracellular PPIX accumulation was conducted through fluorescence-activated cell sorting (FACS), following established procedures [55]. Cancer cells were incubated in medium (outlined in the Section 2.1) containing 1.0 mM ALA at 37 °C for 4 h, under low light conditions. Post-incubation, cells underwent triple washing with Dulbecco's phosphate-buffered saline (DPBS, 1×, Ca^{2+}- and Mg^{2+}-free; Corning, New York, NY, USA, Cat No. 21-031-CV) and were resuspended in 250 µL of 1× DPBS. Subsequently, cells were washed once with serum-free medium (Gibco, Waltham, MA, USA, Cat No. 11835055) and cultured in 6-well plates with the designated medium (described in the Section 2.1), with or without the addition of ALA (0.1 mM, 0.25 mM, 0.5 mM, and 1.0 mM) at 37 °C. Intracellular PPIX concentration was assessed 18 h later using FACS.

The cell suspension of dissociated fibroblasts, pre-treated with a 40 µm Flowmi™ Cell Strainer to exclude clumps and debris, was transferred to BD Falcon tubes under minimal light exposure to mitigate potential phototoxicity from PPIX accumulation.

FACS analyses were executed using a BD LSR II Analyzer (Becton, Dickinson, and Company, Franklin Lakes, NJ, USA) alongside FACSDiva Version 6.1.3 software. To elimi-

nate background red fluorescence, the 633 nm red laser was disabled during PPIX emission data collection. PPIX emission within the 619 nm and 641 nm range (630/22BP filter) was determined following excitation with the 405 nm laser. Forward-scatter (FSC) versus side-scatter (SSC) dot plots were employed to gate the entire cell population, excluding cell debris. A minimum of 10,000 cells within the gated region were then represented in dot plots of SSC vs. PPIX fluorescence, with the gate defined using cells lacking perturbation as negative controls.

2.7. Patient Tumor Gene Expression Analysis and Survival Analysis

We analyzed gene expression data from The Cancer Genome Atlas (TCGA) to investigate the heme biosynthesis process in lung adenocarcinoma and its association with patient survival outcomes. Specifically, we examined the expression levels of ALA dehydratase (ALAD) and hydroxymethylbilane synthase (HMBS), representing the second and third enzymes in the heme biosynthetic pathway, using the TCGA dataset. Kaplan–Meier survival curves [56] and log-rank tests [57] were performed to assess the relationship between gene expression levels and overall survival (OS). Patients were stratified based on high and low gene expression levels, and statistical significance was determined using log-rank tests.

3. Results

3.1. Porphyrin Accumulation Is Present in Lung Cancer Cells

Metabolic dysregulations play an important role in the complex landscape of lung cancer, contributing to its progression, resistance to treatment, and overall clinical outcomes [28–30]. To assess whether lung cancer cells and their tumor microenvironment (TME) overproduce porphyrins, we investigated porphyrin production, characterized by a non-homeostatic or imbalanced heme biosynthetic pathway and heightened accumulation of intermediates.

5-Aminolevulinic acid (ALA) is utilized as a precursor to bypass the rate-limiting first step of heme biosynthesis, facilitating porphyrin accumulation in an unbalanced pathway. When the heme biosynthesis pathway is balanced and there is no porphyrin overdrive, porphyrin accumulation does not occur. Our recent study [38] demonstrated that normal human cells, including primary human liver cells and primary human lung fibroblasts, do not overproduce porphyrins. This finding is consistent with many prior reports [39,58]. In contrast, the human lung cancer cell line H460 readily accumulates protoporphyrin IX (PPIX) after incubation with ALA, indicating characteristics of porphyrin overdrive. High-resolution imaging of human lung cancer H460 cells confirms that PPIX accumulates and is distributed throughout the cell, from mitochondria, where PPIX is synthesized, to the cytosol (Figure 1A).

Results of our analysis of gene expression data for lung cancers and matching normal tissue are illustrated in Figure 1B (Supplemental Table S1). While the expression of *ALAD*, encoding the enzyme for the second step of the heme biosynthetic pathway, is either unaffected or downregulated, the expression of *HMBS*, encoding the third enzyme of the pathway, and the expression of *FLVCR1*, coding for the heme transporter 1, are upregulated in patient tumors (adjusted p value < 0.01). Similarly, the expression of genes for cell differentiation (CAV1 for caveolin-1) [59] and cell proliferation (MKI67 for marker of proliferation Ki-67 and PCNA for proliferating cell nuclear antigen) [60,61] were down- and upregulated, respectively, in tumor samples (adjusted p value < 0.01) (Figure 1B).

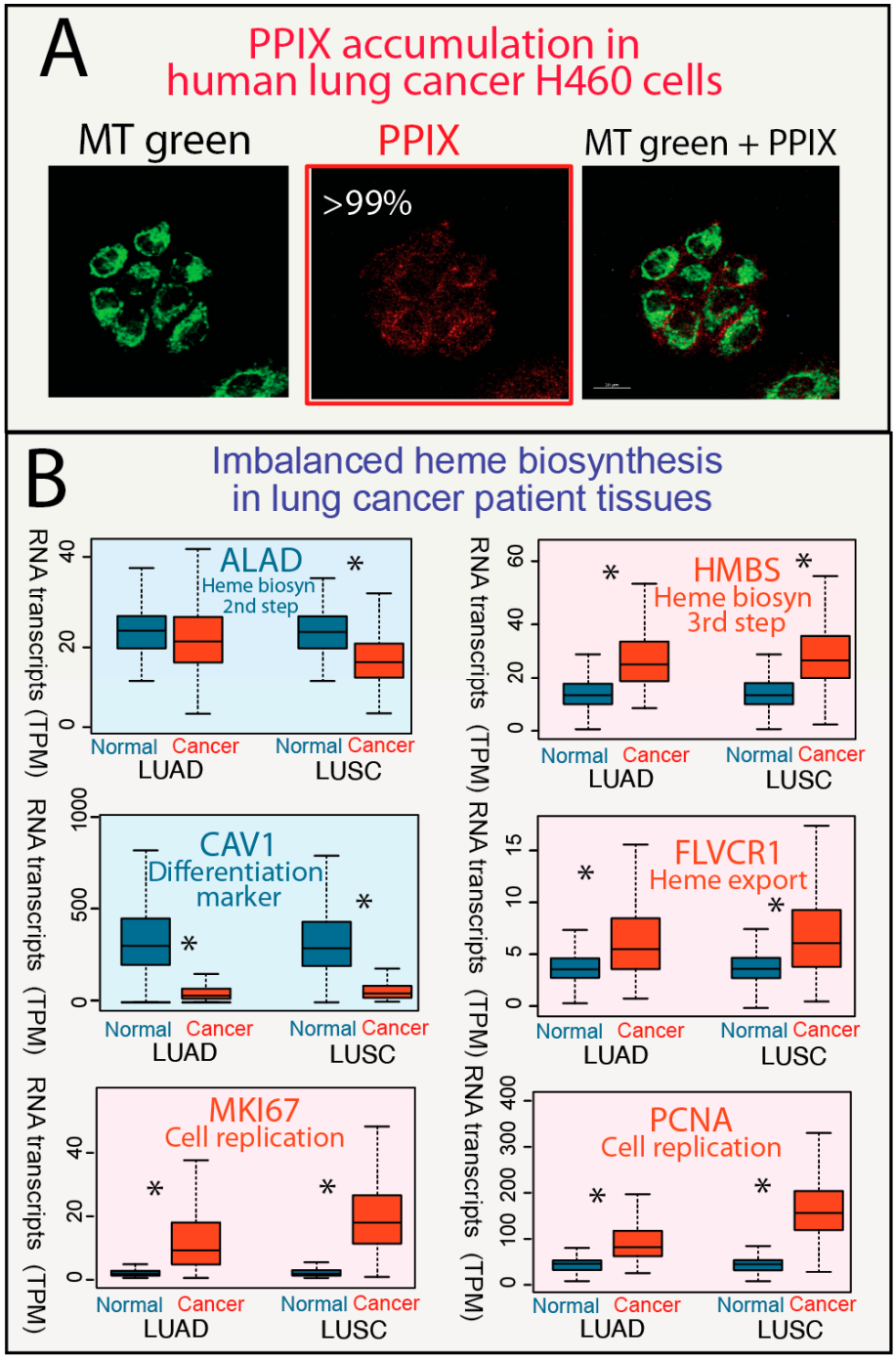

Figure 1. Human lung cancer cells, but not lung fibroblasts, accumulate PPIX. (**A**) After treatment of H460 cells with 1.0 mM ALA for 4 h, the confocal fluorescence images were obtained. From left to right, the panels correspond to (1) green fluorescence, (2) red fluorescence, and (3) superimposed green and red fluorescence images. The green arises from the selective labeling of mitochondria with the MitoTracker Green (MT green) probe (excitation wavelength, λ_{ex}, at 490 nm and emission wavelength, λ_{em}, at 516 nm), and the red fluorescence is due to PPIX fluorescence (λ_{ex} 405 nm; λ_{em}, 635 nm). >99%, over 99% of H460 cells accumulate PPIX. The frame for the pertinent image is colored in red. Scale bars represent 20 μm. (**B**) Gene expression patterns from TCGA lung cancer patients indicate an imbalanced heme biosynthetic pathway and enhanced heme transport. Lung epithelial cell differentiation (CAV1) and cell proliferation (MKI67 and PCNA related genes are plotted as controls. Statistically significant differences are indicated by *) [Abbreviations: DAPI, 4′,6-diamidino-2-phenylindole; LUAD, lung adenocarcinoma; LUSC, lung squamous cell carcinoma].

3.2. CRISPR Analysis Shows Porphyrin Production Contributes to Tumorigenesis

To study the molecular and genetic mechanisms that underlie the reliance of cancer on heme metabolism, we assessed the data from genome-scale CRISPR/Cas9 loss-of-function screens of human lung cancer cell lines. Towards our central focus on the gene dependencies related to the eight enzymatic steps of the heme biosynthetic pathway, we calculated the respective gene essentiality scores, akin to the lethality scores utilized in constructing a cancer dependency map (DepMap) [48–52]. Figure 2 illustrates the survival dependence of 19 metastatic lung cancer cell lines and 28 primary lung cancer cell lines on heme biosynthesis and trafficking. Gene essentiality score values below zero signify a reduction in cell growth/viability upon the loss of gene X. Therefore, the lower the essentiality score of gene X, the greater the dependence of cells on that specific gene (Supplemental Table S2).

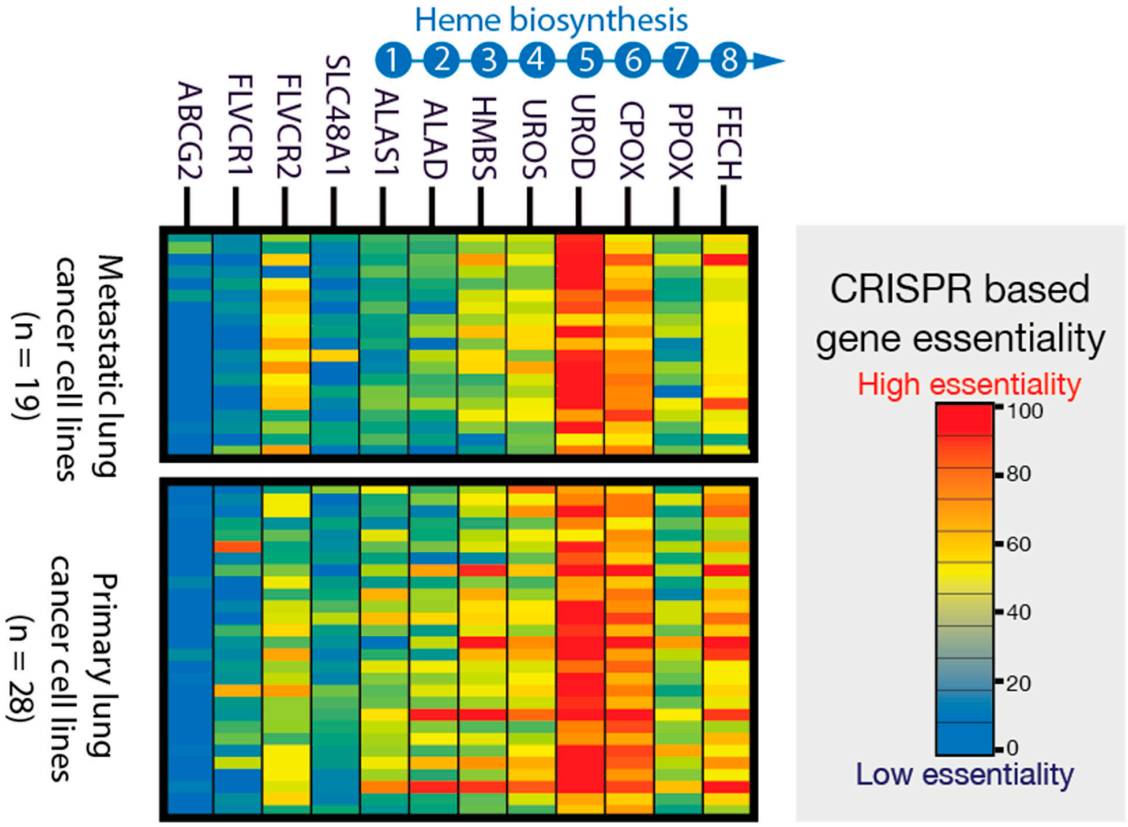

Figure 2. CRISPR/Cas9 gene targeting and inferred gene essentiality in lung cancer cells show porphyrin production. Whole genome loss-of-function growth phenotypes show that a partially functional heme biosynthetic pathway is required to survive. Gene essentiality is estimated from gene X dependency inferred from CRISPR/Cas9 gRNA gene X knockout. Low and high cell viability with deletion of gene X indicate that the cancer cells have a high and low dependence on gene X for survival, respectively. Thus, the lowest and highest gene essentiality values are associated with the least and most profound dependence of the cells on the loss of gene X, respectively. The UROD gene for the fifth enzyme of the pathway has the highest essentiality in cancers, while genes encoding other enzymes are dispensable in many cancer cell lines. Each of the rows represents a distinct cancer cell line derived from primary and metastatic tumors. Numbers 1 to 8 indicate the order of the eight enzymes of the heme biosynthetic pathway. [ABCG2, ATP-binding cassette (ABC) transporter subfamily G, member 2; ALAD, ALA dehydratase (aka porphobilinogen synthase); ALAS1, 5-aminolevulinate synthase 1; CPOX, coproporphyrinogen oxidase; FECH, ferrochelatase; FLVCR, feline leukemia virus subgroup C receptor family; HMBS, hydroxymethylbilane synthase; PPOX, protoporphyrinogen oxidase; SLC48A1, solute carrier family 48, member 1, a.k.a heme transporter HRG1; UROD, uroporphyrinogen III decarboxylase; UROS, uroporphyrinogen III synthase].

Remarkably, instead of encountering the expected fully balanced heme biosynthetic pathway characteristic of normal cells—where all steps exhibit similar essentiality—we observed a cancer cell dependency on various pathway steps in a "non-balanced" manner (Figure 2). Significant genetic essentiality differences were found among genes encoding each step of the pathway (Supplemental Table S3). Specifically, the first step ALAS1 showed no concordance with mid-step genes in essentiality. Notably, the highest cancer gene essentiality was attributed to the genes encoding enzymes responsible for the fifth and sixth steps of the pathway, namely uroporphyrinogen III decarboxylase (UROD) and coproporphyrinogen III oxidae (CPOX), respectively. This lung cancer cell line outcome was consistent with our recent study [38]. These findings reveal the "unbalanced" nature of heme biosynthesis in cancer cells, wherein many cancer cells can survive without functional first and terminal enzymatic steps but demonstrate dependence on the intermediate steps.

Furthermore, the gene essentiality analysis emphasized the significance of heme trafficking, exemplified by the heme importer FLVCR2, in cancer cells for at least in vitro survival (Figure 2). To investigate cancer heme metabolism in vivo, we analyzed previously published in vivo mouse CRISPR/CAS9 loss-of-function and metabolic essentiality data obtained from lung cancer models [53]. Notably, we highlight an increased genetic reliance on these mid-step genes for cancer survival, observed during the transition from in vitro to in vivo conditions, as reported in our recent study [38]. This observation indicates an intensified requirement for the unbalanced pathway of porphyrin accumulation within the tumor tissue environment.

As we have demonstrated in our recent work [38], and consistent with previous findings [53], the gene essentiality data obtained in vivo often differs from that observed in vitro. While the in vitro data may not fully capture the intricacies of tumor biology, both sets of data consistently highlight the essential role of mid-step enzymes in heme biosynthesis. These findings are further supported by the observed accumulation of porphyrins both in vitro and in vivo.

3.3. Porphyrin Production Occurs in Primary Tumor Cancer-Associated Fibroblasts (CAFs) Residing in TME

Remarkably, cancer cells, both in vitro (Figure 2) and in vivo [53], do not necessitate endogenous heme synthesis based on genetic inferences. However, the genes encoding hemoproteins (i.e., proteins requiring heme as a cofactor), such as cytochrome C, are characterized as the top 10% most essential genes [38] in the largest collection of cancer lines in DepMap (version 23Q4), and the heme/intermediates transport gene FLVCR proves to be required (Figure 2). The incongruity observed between the "defect" in endogenous heme production, and the essential requirement for heme cofactors within the cells, indicates the critical nature of trafficking activities. This observation suggests the existence of a specialized cancer microenvironment tailored for efficient metabolite trafficking. Operating within a complex network, cancer cells exhibit a suggested heme flux associated with porphyrin production, characterized by heightened heme and intermediates trafficking. This notion is supported by the genetic dependence on heme trafficking genes (Figure 2) and the elevated expression of trafficking genes in patient tumors (Figure 1C), as seen in the study of the molecular and genetic mechanisms that underlie cancer's reliance on upregulated heme, respectively, in tumor samples (adjusted p value < 0.01) (Figure 1C).

Nevertheless, the source and fate of trafficked heme/porphyrins in the TME remain unclear at present. While heme trafficking is tightly regulated in the normal marrow environment due to potential heme toxicity [55,62,63], the relationship between porphyrin production and the specific cancer microenvironment optimized for heme transport and detoxification remains to be fully elucidated. Of particular interest is the role played by cancer-associated fibroblasts (CAFs), a cell population recognized for its significant contributions to shaping the TME [64]. To study cancer cells and TME at single-cell resolution, we used single-cell lung cancer transcriptomes generated from Zilionis et al. [65] and analyzed heme biosynthesis and trafficking in diverse cell populations present in the

tumor (Supplemental Table S4). HMBS and FLVCR1 were the most upregulated heme biosynthesis genes in tumor cells from three different NSCLC lung cancer patients (Figure 3) (Supplemental Table S4). These single-cell transcriptomes indicate that cancer cells exhibit features of porphyrin production, consistent with the abnormal heme anabolism and endogenous PPIX accumulation upon ALA administration in cancer cells compared to normal cells (Figure 1C). The observed accumulation of porphyrin in cancer cells aligns with existing findings in the literature [39,40,66–71]. Furthermore, the clinical advancement of photodynamic therapy for lung cancer [72–74], which leverages the light properties of cancer porphyrins, offers additional clinical evidence of porphyrin accumulation in lung cancer cells. By contrast, major groups of stromal and immune cell populations do not show evidence of imbalanced heme biosynthesis or heme trafficking (Figure 3).

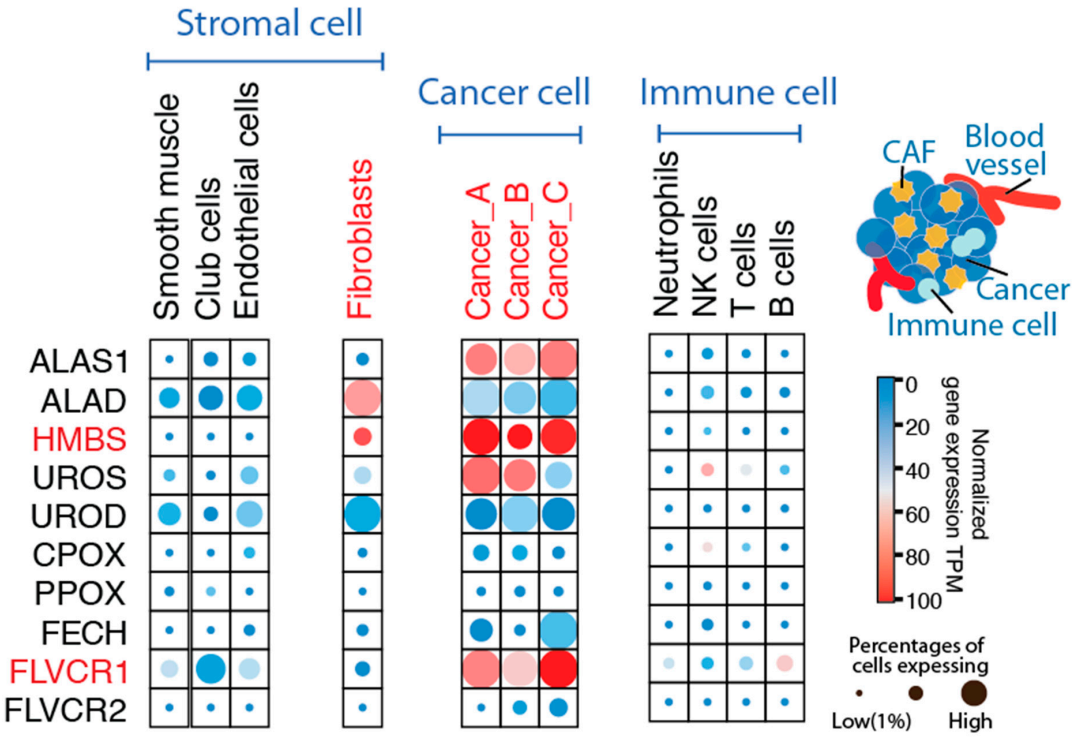

Figure 3. Single-cell RNA sequencing of cells from human lung cancer patients supports non-homeostatic porphyrin production in cancer-associated fibroblasts. The data on single-cell lung cancer transcriptomes were retrieved from Zilionis et al. [65]. The expression of the genes for the heme biosynthetic pathway enzymes and heme trafficking proteins was analyzed in diverse cell populations present in the tumor. The expression results associated with cancer cells from three different patients (Cancer_A n = 203 cells, Cancer_B n = 766 cells, and Cancer_C n = 538 cells) are plotted—*HMBS* and *FLVCR1* show the most upregulated gene expression patterns. In the major groups of stromal and immune cell populations, most cell types have no evidence of porphyrin accumulation, while cancer-associated fibroblasts (n = 585) show evidence of porphyrin production with upregulation of *HMBS* ($p < 0.05$). Both *HMBS* and *FLVCR1* are significantly different between tumor and stromal cell populations ($p < 0.05$). Color shading indicates normalized gene expression levels per gene, in a given cell population, and circle sizes indicate the percentage of cells in that population with detectable single-cell transcriptomes.

In cancer, porphyrin production is likely fostered by the specific TME, including CAFs [64]. Our single-cell RNAseq analysis revealed that lung cancer-associated fibroblasts (CAFs) exhibit characteristics indicative of porphyrin production, with significantly upregulated HMBS gene expression ($p < 0.01$) compared to other stromal components (Figure 3). Consistent with our previous findings [38] and the current data depicted in Figure 1B and Figure 5, HMBS emerges as a key indicator of in vivo porphyrin accumulation. These

results collectively support the hypothesis that dysregulation of HMBS plays a pivotal role in driving porphyrin accumulation within the tumor microenvironment (Figure 3).

Next, we provide the experimental validation that porphyrin production operates in CAFs derived from primary tumors from a lung adenocarcinoma patient, as assessed by PPIX quantification. The tumor is derived from treatment-naïve patient samples (female, 55 years, TNM Staging: T2N0M0). The samples were obtained from surgically excised tissues, and the CAFs were isolated (BioIVT). Immunohistochemical staining for Vimentin revealed that over 95% of isolated cells within the tumor are positive for Vimentin, indicating a significant presence of mesenchymal characteristics. We show that CAFs from primary lung adenocarcinoma accumulate heme intermediates (e.g., PPIX) upon induction with ALA, a precursor substrate of the heme biosynthetic pathway (Figure 4A), but they lose this feature when the CAFs are passaged in vitro for over 15 generations (Figure 4B). Interestingly, the fibroblasts adjacent to the tumor also show porphyrin overdrive, albeit to a lesser extent ("CAF vs. Other fibroblasts adjacent to tumor") (Figure 4B). These findings suggest that TME acts as a continuum of aberrant heme metabolism.

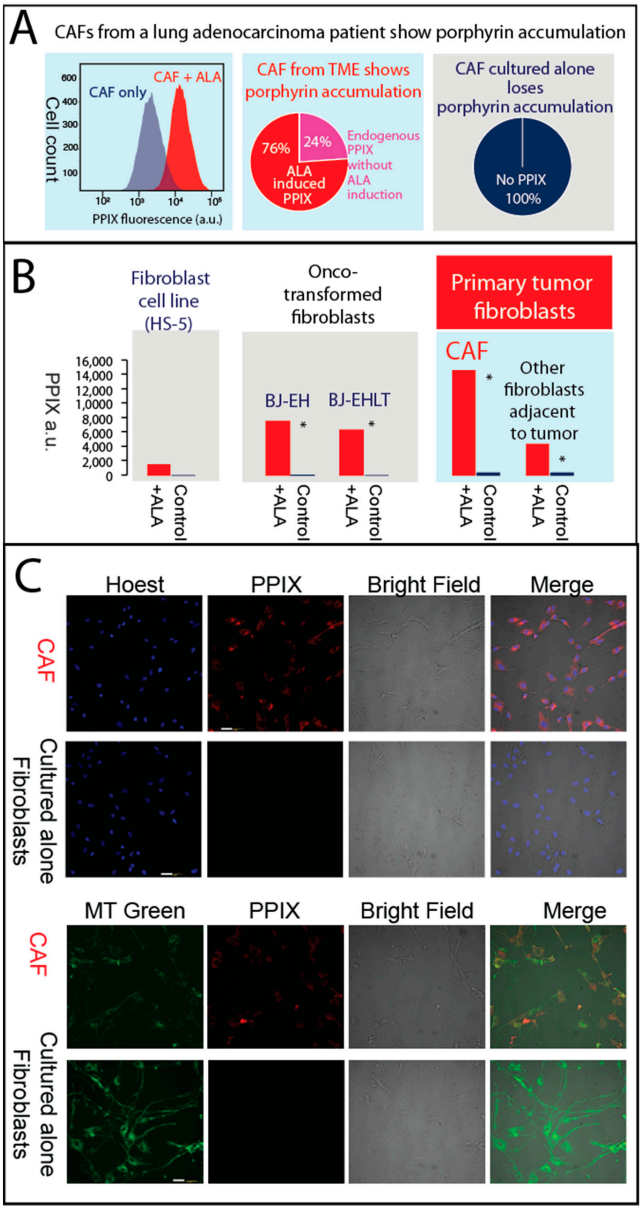

Figure 4. Primary CAFs accumulate PPIX. (**A**) The primary tumor is primary lung adenocarcinoma. ALA (1 mM final concentration) was added at least 4 h prior to flowcytometry and PPIX quantification.

Normalized CAFs, after 15 in vitro passages from the same lung cancer patient, maintained rigorous cell growth and cell division but lost porphyrin production entirely (**right panel**). Porphyrin production, as estimated from PPIX accumulation, is present in over 99% of CAFs from primary lung adenocarcinoma (**left panel**). Even without ALA induction, PPIX accumulates in 24% of the CAFs (middle panel). (**B**) Primary CAFs, onco-transformed fibroblasts, and cancer cells show similar patterns of ALA induced PPIX. * Indicates significant differences. (**C**) Primary CAFs accumulate PPIX, while cultured alone, they cease accumulation. After treatment of CAFs and fibroblasts cultured alone (CAFs after culture passages) with 1.0 mM ALA for 4 h, confocal fluorescence images were obtained. From left to right, the panels correspond to (1) blue fluorescence or green fluorescence, (2) red fluorescence, (3) bright field, and (4) superimposed fluorescence images. The blue arises from nuclear staining with Hoechst, the green from selective labeling of mitochondria with the MitoTracker Green (MT green) probe (excitation wavelength, λex at 490 nm and emission wavelength, λem at 516 nm), and the red fluorescence is due to PPIX fluorescence (λex 405 nm; λem, 635 nm). Over 99% of H460 cells accumulate PPIX. Scale bars represent 50 μm.

We performed high-resolution imaging to validate our flow cytometry data, confirming that PPIX accumulates and is dispersed throughout the CAFs, starting from the mitochondria where PPIX is synthesized and extending to the cytosol (Figure 4C). By contrast, 0% of the tested fibroblasts cultured alone (CAFs after culture passages) accumulate PPIX after the addition of exogenous ALA (Figure 4C), indicating balanced heme biosynthesis and lack of porphyrin overdrive.

In sum, our experiments show that the lung cancer TME exhibits characteristics of porphyrin production, based on single-cell RNAseq analysis and our experimental validation with CAFs isolated from a treatment-naïve lung adenocarcinoma patient.

3.4. Porphyrin Overproduction Is Elevated in More Aggressive Cancers and Linked to Overall Survival of Patients

To evaluate the clinical relevance of porphyrin overdrive in lung cancers, we studied both patient tumor tissues from TCGA [45,47] and analyzed previously generated single-cell RNAseq data [65]. For human tissue gene expression in patient lung tumors, *HMBS* and *FLVCR1* are the most enriched expressed genes, as compared to normal tissues (Figure 5A). For the single-cell transcriptomes, we used the single-cell expression data from Zilionis et al. [65] and examined the expression differences in more aggressive vs. more differentiated lung cancer cell populations within the same tumor. Our results show both combined data of patient tumors (Figure 5A) and single cancer cells show evidence of porphyrin production (Figure 5B).

To further illustrate the increased skewness in the linear biosynthesis pathway, indicative of a higher degree of intermediate accumulation (porphyrin overdrive), we analyzed the gene expression ratio between *ALAD* and *HMBS* (Figure 5C). Our findings reveal that lung cancer patient samples exhibit an aberrant ratio, suggesting unbalanced enzyme production. Similarly, the ratio between the heme/porphyrin exporter *FLVCR1* and importer *FLVCR2* genes (Figure 5D) indicates enhanced exporting function in lung cancers.

We next analyzed overall survival with respect to high and low expression of the mid-step heme biosynthesis genes, *ALAD* and *HMBS*, using data from TCGA [47]. ALAD (the enzyme responsible for the second step of heme biosynthesis) and HMBS (the enzyme that catalyzes the third step) show contrasting prognostic results in overall survival, indicating the more imbalanced the porphyrin production (the larger the differences between ALAD and HMBS expression), the poorer the overall patient survival (Figure 5E,F).

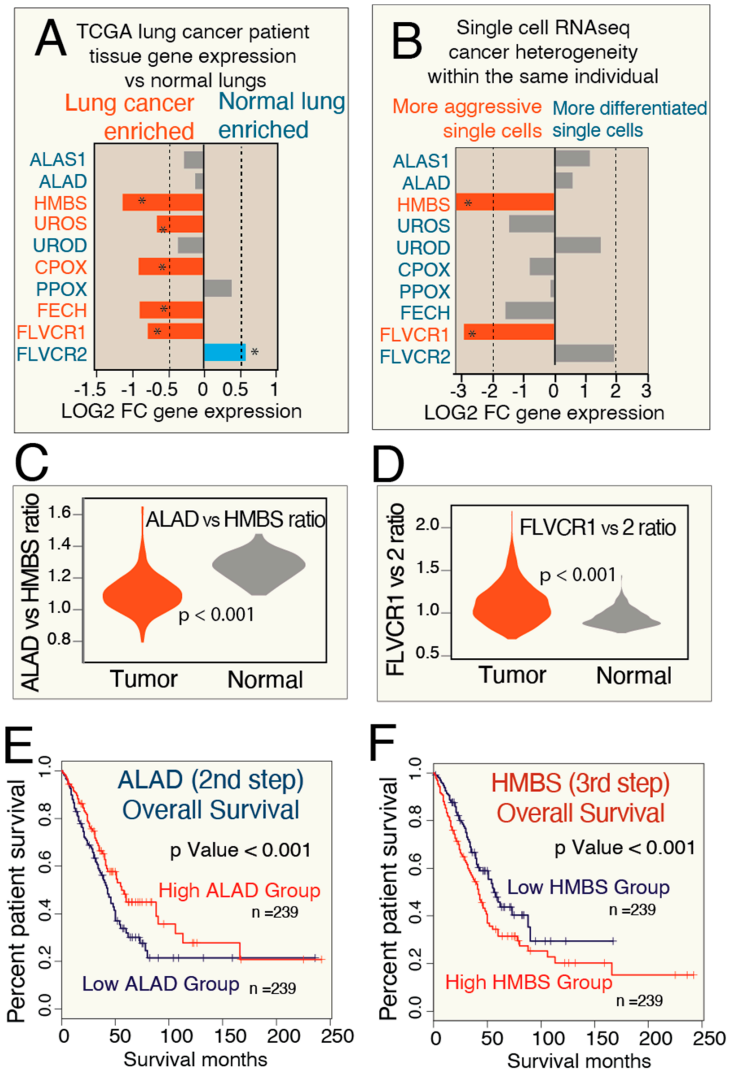

Figure 5. Lung cancer imbalanced heme biosynthesis is supported by both bulk and single-cell RNAseq and is linked to the overall survival (OS) of patients. (**A**,**B**) Patient tumor tissue RNAseq and single-cell lung cancer RNAseq support porphyrin overdrive. Genome analysis (shown in (**A**)) was based on lung cancer data publicly available at The Cancer Genome Atlas (TGCA) and Genotype-Tissue Expression (GTEx) program. The single-cell expression data from Zilionis et al. [65] were used to study the expression differences in more aggressive vs. more differentiated lung cancer cell populations within the same tumor. * denotes statistically significant differences ($p < 0.05$). (**C**) The skewness of the heme biosynthesis pathway, representing the degree of porphyrin overdrive, is quantified by the ratio of ALAD to HMBS expression levels. (**D**) The disparity in expression levels between the heme/porphyrin export gene FLVCR1 and the importer FLVCR2 is determined by the ratio of these two genes. (**E**,**F**) Imbalanced heme biosynthesis in lung cancer is related to patient OS. The Kaplan–Meier estimator, a non-parametric statistic, was used to estimate the survival function from the lifetime data. Shown are the Kaplan–Meier curves for data of visualization of *ALAD* (panel (**C**)) and *HMBS* expression (panel (**D**)) in lung adeno carcinoma cancer patients. The expression data were from TCGA and were analyzed in relation to the OS of the respective patients. Expression of *ALAD* and *HMBS* (the genes for the second and third enzymes of the heme biosynthetic pathway, respectively) show contrasting prognostic results in patients' OS, suggesting that the greater the extent of porphyrin production (i.e., the larger the difference between ALAD and HMBS expression), the more aggressive the lung cancer. The statistical difference between the groups is estimated by the log-rank test. [FC, fold-change]. Tumor or more aggressive tumor results are colored red.

4. Discussion

TME is a dynamic milieu, orchestrating various cellular and molecular components. Dysregulated metabolisms within the TME have emerged as pivotal players in cancer progression, contributing to diagnostic nuances and therapeutic potential [75]. Metabolic shifts, such as the Warburg effect, heightened glutamine metabolism, altered lipid metabolism, perturbed one-carbon metabolism, and disrupted redox homeostasis, represent different aspects of metabolic rewiring in cancer [5,6]. Our study introduces a novel facet of this metabolic landscape by delineating the dysregulation in heme biosynthesis, specifically the aberrant production of porphyrins, within the TME. The dysregulated heme metabolism, in the form of porphyrin overproduction of both cancer cells and CAFs, suggests potential therapeutic vulnerabilities.

Notably, CAFs, recognized for their influential role in shaping the TME [6,64], contribute to porphyrin production. The experimental validation of porphyrin accumulation in CAFs from primary lung adenocarcinoma emphasizes the contributions of different stromal players of aberrant heme metabolism within the TME. These findings suggest that the TME acts as a specialized microenvironment, fostering porphyrin production and influencing the overall metabolic landscape of cancer. The precise molecular pathways and trafficking routes of porphyrins within the TME is yet to be determined.

The unexpected non-balanced reliance on intermediate steps of heme biosynthesis, as opposed to the initial and terminal steps, challenges conventional assumptions. We recently reported this process as "Porphyrin Overdrive" [38], and suggested it as a novel therapeutic target. Importantly, cancer cells exhibit a heightened dependence on mid-step enzyme genes, emphasizing the unbalanced nature of heme biosynthesis. This genetic vulnerability opens avenues for targeted therapeutic interventions. The significance of heme trafficking genes offers potential targets for therapeutic strategies aimed at disrupting cancer-specific metabolic trafficking as a treatment to be developed.

Cancers are diseases of the tissues [76,77]. Thus, cancers can be viewed as an emergent phenomenon where their properties extend beyond their individual stromal components. Despite the recognized high genetic heterogeneity and exceedingly diverse cell populations within the TME [78–80], our research on porphyrin overdrive offers another perspective by highlighting the unifying features of the TME, which we propose as "Niche Convergence", defined in terms of shared features of onco-metabolism and intracellular communications. We propose that tumors exhibit a set of strikingly shared metabolic and redox properties.

We present three lines of evidence to support the proposal of tumor niche convergence. First, we highlight the correlation between aberrant tumor glycolysis (i.e., the Warburg effect) [7,8,81] and tumor development. PET imaging, based on enhanced glucose uptake and considered the gold standard in clinical cancer imaging [81–83], can track tumor progression [76], indicating patterns of metabolic rewiring exist in the TME. Second, the clinical application of porphyrin overdrive by detecting porphyrin accumulation in multiple tumor types for diagnosis and grading [66–69,84], particularly in surgical procedures for high-grade brain tumors [85], indicates that porphyrin overdrive can be used to distinguish and surgically excise vastly different tumors in vivo. Third, we propose a link between the dysregulated redox properties of tumors and longstanding evidence that tumors share depolarized cell plasma membrane potentials [86–88], indicating aberrant bioelectric properties at the interface of tumor cells with their TME. We hypothesize that porphyrins, as redox-active molecules [69,89], may disrupt cell redox homeostasis or signaling across diverse tumors, thereby fostering collaboration between tumor and stromal cells to shape the TME environment. Future work will help elucidate common features of the tumor niche for therapy development.

Lung cancer is a pervasive global health concern, and this type of cancer exhibits profound metabolic dysregulations that significantly impact its clinical outcomes [90,91]. This study shows the absence of porphyrin accumulation in normal cells, in stark contrast to the presence of porphyrins in lung cancer cells. The evidence of porphyrin production in TME, as verified in lung adenocarcinoma, provides crucial insights into the metabolic

rewiring of TME components associated with tumorigenesis. The clinical implications of porphyrin production in lung cancers extend beyond diagnostic considerations. The examination of patient tumor tissues and single-cell RNAseq data shows the association of porphyrin production with more aggressive cancers. High expression of mid-step heme biosynthesis genes correlates with overall poorer survival outcomes in lung cancer patients. This prognostic relevance establishes porphyrin production as a potential biomarker for predicting cancer aggressiveness and clinical progression. The integration of these findings into clinical practice holds the promise of refining prognostic assessments and tailoring therapeutic strategies based on the metabolic nuances observed in individual cancer cases.

5. Conclusions

Our investigation highlights a distinct facet of cancer metabolism characterized by the overproduction of porphyrins within tumors and their microenvironments. This aberrant porphyrin production, evident in both cancer cells and stromal components of the tumor microenvironment (TME), introduces a new dimension to the metabolic interplay of tumorigenesis. The exclusive presence of porphyrin overproduction in tumors and the TME, absent in normal tissues, demonstrates its potential as a novel therapeutic target. Additionally, porphyrin overproduction emerges as a promising prognostic indicator of cancer aggressiveness and clinical outcomes, suggesting avenues for innovative anti-tumor therapies aimed at disrupting metabolic interactions within the TME.

Supplementary Materials: The following supporting information can be downloaded at: https://www.mdpi.com/article/10.3390/genes15070961/s1, Supplemental Table S1: Expression differences between lung cancer and normal tissues. Supplemental Table S1: CRISPR essentiality data for heme biosynthesis and heme related trafficking genes in lung cancer cell lines. Supplemental Table S3: Lack of CRISPR essentiality score between different steps of genes encoding the heme biosynthesis enzymes. Supplemental Table S4: scRNAseq lung cancer cluster gene expression percentages and levels.

Author Contributions: Conceptualization, S.R.A. and R.H.Y.J.; Methodology, S.R.A. and R.H.Y.J.; Formal analysis, R.H.Y.J.; Investigation, S.R.A., A.S., P.M. and R.H.Y.J.; Writing—original draft, G.C.F. and R.H.Y.J.; Supervision, G.C.F. and R.H.Y.J.; Project administration, S.R.A.; Funding acquisition, R.H.Y.J. All authors have read and agreed to the published version of the manuscript.

Funding: R.H.Y.J., S.R.A and G.C.F have received Florida Department of Health grant support 9BC14, to perform part of the research. R.H.Y.J. also received WLP (Women's Leadership and Philanthropy) award support during research and writing of the work. Genetic onco-transformed fibroblasts were kindly provided by Robert Weinberg at MIT.

Institutional Review Board Statement: Not applicable.

Informed Consent Statement: Not applicable.

Data Availability Statement: The original contributions presented in the study are included in the article/Supplementary Material, further inquiries can be directed to the corresponding author/s.

Conflicts of Interest: The authors declare no conflicts of interest.

References

1. Sung, H.; Ferlay, J.; Siegel, R.L.; Laversanne, M.; Soerjomataram, I.; Jemal, A.; Bray, F. Global Cancer Statistics 2020: GLOBOCAN Estimates of Incidence and Mortality Worldwide for 36 Cancers in 185 Countries. *CA Cancer J. Clin.* **2021**, *71*, 209–249. [CrossRef]
2. Giraldo, N.A.; Sanchez-Salas, R.; Peske, J.D.; Vano, Y.; Becht, E.; Petitprez, F.; Validire, P.; Ingels, A.; Cathelineau, X.; Fridman, W.H.; et al. The clinical role of the TME in solid cancer. *Br. J. Cancer* **2019**, *120*, 45–53. [CrossRef]
3. Anderson, N.M.; Simon, M.C. The tumor microenvironment. *Curr. Biol.* **2020**, *30*, R921–R925. [CrossRef]
4. Elia, I.; Haigis, M.C. Metabolites and the tumour microenvironment: From cellular mechanisms to systemic metabolism. *Nat. Metab.* **2021**, *3*, 21–32. [CrossRef]
5. Binnewies, M.; Roberts, E.W.; Kersten, K.; Chan, V.; Fearon, D.F.; Merad, M.; Coussens, L.M.; Gabrilovich, D.I.; Ostrand-Rosenberg, S.; Hedrick, C.C.; et al. Understanding the tumor immune microenvironment (TIME) for effective therapy. *Nat. Med.* **2018**, *24*, 541–550. [CrossRef]
6. Naser, R.; Fakhoury, I.; El-Fouani, A.; Abi-Habib, R.; El-Sibai, M. Role of the tumor microenvironment in cancer hallmarks and targeted therapy (Review). *Int. J. Oncol.* **2023**, *62*, 1–28. [CrossRef]

7. Wang, Y.; Patti, G.J. The Warburg effect: A signature of mitochondrial overload. *Trends Cell Biol.* **2023**, *33*, 1014–1020. [CrossRef]
8. Liberti, M.V.; Locasale, J.W. The Warburg Effect: How Does it Benefit Cancer Cells? *Trends Biochem. Sci.* **2016**, *41*, 211–218. [CrossRef]
9. Zhang, J.; Pavlova, N.N.; Thompson, C.B. Cancer cell metabolism: The essential role of the nonessential amino acid, glutamine. *Embo J.* **2017**, *36*, 1302–1315. [CrossRef]
10. Broadfield, L.A.; Pane, A.A.; Talebi, A.; Swinnen, J.V.; Fendt, S.M. Lipid metabolism in cancer: New perspectives and emerging mechanisms. *Dev. Cell* **2021**, *56*, 1363–1393. [CrossRef]
11. Currie, E.; Schulze, A.; Zechner, R.; Walther, T.C.; Farese, R.V., Jr. Cellular fatty acid metabolism and cancer. *Cell Metab.* **2013**, *18*, 153–161. [CrossRef]
12. Ducker, G.S.; Rabinowitz, J.D. One-Carbon Metabolism in Health and Disease. *Cell Metab.* **2017**, *25*, 27–42. [CrossRef]
13. Yang, M.; Vousden, K.H. Serine and one-carbon metabolism in cancer. *Nat. Rev. Cancer* **2016**, *16*, 650–662. [CrossRef]
14. Locasale, J.W. Serine, glycine and one-carbon units: Cancer metabolism in full circle. *Nat. Rev. Cancer* **2013**, *13*, 572–583. [CrossRef] [PubMed]
15. Jiang, X.; Stockwell, B.R.; Conrad, M. Ferroptosis: Mechanisms, biology and role in disease. *Nat. Rev. Mol. Cell Biol.* **2021**, *22*, 266–282. [CrossRef]
16. Vicente, M.D.; Smith, K.M. Syntheses and Functionalizations of Porphyrin Macrocycles. *Curr. Org. Synth.* **2014**, *11*, 3–28. [CrossRef] [PubMed]
17. Menezes, J.C.J.M.D.S.; Faustino, M.A.F.; de Oliveira, K.T.; Uliana, M.P.; Ferreira, V.F.; Hackbarth, S.; Röder, B.; Teixeira Tasso, T.; Furuyama, T.; Kobayashi, N.; et al. Synthesis of New Chlorin e6 Trimethyl and Protoporphyrin IX Dimethyl Ester Derivatives and Their Photophysical and Electrochemical Characterizations. *Chem. A Eur. J.* **2014**, *20*, 13644–13655. [CrossRef] [PubMed]
18. Das, M.; Srinivasan, A. Advent and features of pyriporphyrinoids: An overview of a pyridine-based porphyrin analogue. *Chem. Commun.* **2023**, *59*, 11780–11790. [CrossRef] [PubMed]
19. Tahoun, M.; Gee, C.T.; McCoy, V.E.; Sander, P.M.; Müller, C.E. Chemistry of porphyrins in fossil plants and animals. *RSC Adv.* **2021**, *11*, 7552–7563. [CrossRef]
20. Shimizu, T.; Lengalova, A.; Martínek, V.; Martínková, M. Heme: Emergent roles of heme in signal transduction, functional regulation and as catalytic centres. *Chem. Soc. Rev.* **2019**, *48*, 5624–5657. [CrossRef]
21. Kato, H.; Itoh-Nakadai, A.; Matsumoto, M.; Ishii, Y.; Watanabe-Matsui, M.; Ikeda, M.; Ebina-Shibuya, R.; Sato, Y.; Kobayashi, M.; Nishizawa, H.; et al. Infection perturbs Bach2- and Bach1-dependent erythroid lineage 'choice' to cause anemia. *Nat. Immunol.* **2018**, *19*, 1059–1070. [CrossRef] [PubMed]
22. Nishinaga, M.; Sugimoto, H.; Nishitani, Y.; Nagai, S.; Nagatoishi, S.; Muraki, N.; Tosha, T.; Tsumoto, K.; Aono, S.; Shiro, Y.; et al. Heme controls the structural rearrangement of its sensor protein mediating the hemolytic bacterial survival. *Commun. Biol.* **2021**, *4*, 467. [CrossRef] [PubMed]
23. Zheng, H.; Williams, J.T.; Aleiwi, B.; Ellsworth, E.; Abramovitch, R.B. Inhibiting *Mycobacterium tuberculosis* DosRST Signaling by Targeting Response Regulator DNA Binding and Sensor Kinase Heme. *ACS Chem. Biol.* **2020**, *15*, 52–62. [CrossRef] [PubMed]
24. Hoque, N.J.; Weinert, E.E. Control of bacterial second messenger signaling and motility by heme-based direct oxygen-sensing proteins. *Curr. Opin. Microbiol.* **2023**, *76*, 102396. [CrossRef] [PubMed]
25. Quick-Cleveland, J.; Jacob, J.P.; Weitz, S.H.; Shoffner, G.; Senturia, R.; Guo, F. The DGCR8 RNA-binding heme domain recognizes primary microRNAs by clamping the hairpin. *Cell Rep.* **2014**, *7*, 1994–2005. [CrossRef] [PubMed]
26. Chen, J.-J.; Zhang, S. Heme-regulated eIF2α kinase in erythropoiesis and hemoglobinopathies. *Blood* **2019**, *134*, 1697–1707. [CrossRef] [PubMed]
27. Zenke-Kawasaki, Y.; Dohi, Y.; Katoh, Y.; Ikura, T.; Ikura, M.; Asahara, T.; Tokunaga, F.; Iwai, K.; Igarashi, K. Heme induces ubiquitination and degradation of the transcription factor Bach1. *Mol. Cell Biol.* **2007**, *27*, 6962–6971. [CrossRef]
28. Carter, E.L.; Gupta, N.; Ragsdale, S.W. High Affinity Heme Binding to a Heme Regulatory Motif on the Nuclear Receptor Rev-erbβ Leads to Its Degradation and Indirectly Regulates Its Interaction with Nuclear Receptor Corepressor. *J. Biol. Chem.* **2016**, *291*, 2196–2222. [CrossRef]
29. Yang, J.; Kim, K.D.; Lucas, A.; Drahos, K.E.; Santos, C.S.; Mury, S.P.; Capelluto, D.G.; Finkielstein, C.V. A novel heme-regulatory motif mediates heme-dependent degradation of the circadian factor period 2. *Mol. Cell Biol.* **2008**, *28*, 4697–4711. [CrossRef]
30. Yi, L.; Morgan, J.T.; Ragsdale, S.W. Identification of a thiol/disulfide redox switch in the human BK channel that controls its affinity for heme and CO. *J. Biol. Chem.* **2010**, *285*, 20117–20127. [CrossRef]
31. Fleischhacker, A.S.; Carter, E.L.; Ragsdale, S.W. Redox Regulation of Heme Oxygenase-2 and the Transcription Factor, Rev-Erb, Through Heme Regulatory Motifs. *Antioxid. Redox Signal.* **2018**, *29*, 1841–1857. [CrossRef]
32. Motomura, T.; Suga, M.; Hienerwadel, R.; Nakagawa, A.; Lai, T.L.; Nitschke, W.; Kuma, T.; Sugiura, M.; Boussac, A.; Shen, J.R. Crystal structure and redox properties of a novel cyanobacterial heme protein with a His/Cys heme axial ligation and a Per-Arnt-Sim (PAS)-like domain. *J. Biol. Chem.* **2017**, *292*, 9599–9612. [CrossRef] [PubMed]
33. Hunter, G.A.; Al-Karadaghi, S.; Ferreira, G.C. Ferrochelatase: The convergence of the porphyrin biosynthesis and iron transport pathways. *J. Porphyr. Phthalocyanines* **2011**, *15*, 350–356. [CrossRef] [PubMed]
34. Hunter, G.A.; Ferreira, G.C. Metal ion coordination sites in ferrochelatase. *Coord. Chem. Rev.* **2022**, *460*, 214464. [CrossRef]
35. Yien, Y.Y.; Perfetto, M. Regulation of Heme Synthesis by Mitochondrial Homeostasis Proteins. *Front. Cell Dev. Biol.* **2022**, *10*, 895521. [CrossRef] [PubMed]

36. Kozlowski, H.; Kolkowska, P.; Watly, J.; Krzywoszynska, K.; Potocki, S. General aspects of metal toxicity. *Curr. Med. Chem.* **2014**, *21*, 3721–3740. [CrossRef] [PubMed]
37. Qi, Q.; Gu, R.; Zhu, J.; Anderson, K.E.; Ma, X. Roles of the ABCG2 transporter in protoporphyrin IX distribution and toxicity. *Drug Metab. Dispos.* **2024**, *52*, 1582. [CrossRef] [PubMed]
38. Adapa, S.R.; Hunter, G.A.; Amin, N.E.; Marinescu, C.; Borsky, A.; Sagatys, E.M.; Sebti, S.M.; Reuther, G.W.; Ferreira, G.C.; Jiang, R.H.Y. Porphyrin overdrive rewires pan-cancer cell metabolism. *Life Sci. Alliances*, 2023; *in press*. [CrossRef]
39. Berg, K.; Selbo, P.K.; Weyergang, A.; Dietze, A.; Prasmickaite, L.; Bonsted, A.; Engesaeter, B.; Angell-Petersen, E.; Warloe, T.; Frandsen, N.; et al. Porphyrin-related photosensitizers for cancer imaging and therapeutic applications. *J. Microsc.* **2005**, *218*, 133–147. [CrossRef]
40. Gomes, A.; Neves, M.; Cavaleiro, J.A.S. Cancer, Photodynamic Therapy and Porphyrin-Type Derivatives. *An. Acad. Bras. Cienc.* **2018**, *90*, 993–1026. [CrossRef]
41. Wang, T.; Ashrafi, A.; Konduri, P.C.; Ghosh, P.; Dey, S.; Modareszadeh, P.; Salamat, N.; Alemi, P.S.; Berisha, E.; Zhang, L. Heme Sequestration as an Effective Strategy for the Suppression of Tumor Growth and Progression. *Mol. Cancer Ther.* **2021**, *20*, 2506–2518. [CrossRef]
42. Sohoni, S.; Ghosh, P.; Wang, T.; Kalainayakan, S.P.; Vidal, C.; Dey, S.; Konduri, P.C.; Zhang, L. Elevated Heme Synthesis and Uptake Underpin Intensified Oxidative Metabolism and Tumorigenic Functions in Non-Small Cell Lung Cancer Cells. *Cancer Res.* **2019**, *79*, 2511–2525. [CrossRef]
43. Kiening, M.; Lange, N. A Recap of Heme Metabolism towards Understanding Protoporphyrin IX Selectivity in Cancer Cells. *Int. J. Mol. Sci.* **2022**, *23*, 7974. [CrossRef] [PubMed]
44. Fiorito, V.; Allocco, A.L.; Petrillo, S.; Gazzano, E.; Torretta, S.; Marchi, S.; Destefanis, F.; Pacelli, C.; Audrito, V.; Provero, P.; et al. The heme synthesis-export system regulates the tricarboxylic acid cycle flux and oxidative phosphorylation. *Cell Rep.* **2021**, *35*, 109252. [CrossRef] [PubMed]
45. Ardlie, K. The Genotype-Tissue Expression (GTEx) pilot analysis: Multitissue 1252 gene regulation in humans. *Science* **2015**, *348*, 648–660.
46. Lonsdale, J.; Thomas, J.; Salvatore, M.; Phillips, R.; Lo, E.; Shad, S.; Hasz, R.; Walters, G.; Garcia, F.; Young, N.; et al. The Genotype-Tissue Expression (GTEx) project. *Nat. Genet.* **2013**, *45*, 580–585. [CrossRef] [PubMed]
47. Chang, K.; Creighton, C.J.; Davis, C.; Donehower, L.; Drummond, J.; Wheeler, D.; Ally, A.; Balasundaram, M.; Birol, I.; Butterfield, Y.S.N.; et al. The Cancer Genome Atlas Pan-Cancer analysis project. *Nat. Genet.* **2013**, *45*, 1113–1120. [CrossRef]
48. Aguirre, A.J.; Meyers, R.M.; Weir, B.A.; Vazquez, F.; Zhang, C.-Z.; Ben-David, U.; Cook, A.; Ha, G.; Harrington, W.F.; Doshi, M.B.; et al. Genomic Copy Number Dictates a Gene-Independent Cell Response to CRISPR/Cas9 Targeting. *Cancer Discov.* **2016**, *6*, 914–929. [CrossRef]
49. Kim, E.; Hart, T. Improved analysis of CRISPR fitness screens and reduced off-target effects with the BAGEL2 gene essentiality classifier. *Genome Med.* **2021**, *13*, 2. [CrossRef]
50. Meyers, R.M.; Bryan, J.G.; McFarland, J.M.; Weir, B.A.; Sizemore, A.E.; Xu, H.; Dharia, N.V.; Montgomery, P.G.; Cowley, G.S.; Pantel, S.; et al. Computational correction of copy number effect improves specificity of CRISPR-Cas9 essentiality screens in cancer cells. *Nat. Genet.* **2017**, *49*, 1779–1784. [CrossRef]
51. Dempster, J.M.; Pacini, C.; Pantel, S.; Behan, F.M.; Green, T.; Krill-Burger, J.; Beaver, C.M.; Younger, S.T.; Zhivich, V.; Najgebauer, H.; et al. Agreement between two large pan-cancer CRISPR-Cas9 gene dependency data sets. *Nat. Commun.* **2019**, *10*, 5817. [CrossRef]
52. Pacini, C.; Dempster, J.M.; Boyle, I.; Gonçalves, E.; Najgebauer, H.; Karakoc, E.; van der Meer, D.; Barthorpe, A.; Lightfoot, H.; Jaaks, P.; et al. Integrated cross-study datasets of genetic dependencies in cancer. *Nat. Commun.* **2021**, *12*, 1661. [CrossRef]
53. Zhu, X.G.; Chudnovskiy, A.; Baudrier, L.; Prizer, B.; Liu, Y.; Ostendorf, B.N.; Yamaguchi, N.; Arab, A.; Tavora, B.; Timson, R.; et al. Functional Genomics In Vivo Reveal Metabolic Dependencies of Pancreatic Cancer Cells. *Cell Metab.* **2021**, *33*, 211–221.e6. [CrossRef]
54. Sattabongkot, J.; Yimamnuaychoke, N.; Leelaudomlipi, S.; Rasameesoraj, M.; Jenwithisuk, R.; Coleman, R.E.; Udomsangpetch, R.; Cui, L.; Brewer, T.G. Establishment of a human hepatocyte line that supports in vitro development of the exo-erythrocytic stages of the malaria parasites Plasmodium falciparum and P. vivax. *Am. J. Trop. Med. Hyg.* **2006**, *74*, 708–715. [CrossRef]
55. Fratz, E.J.; Hunter, G.A.; Ferreira, G.C. Expression of Murine 5-Aminolevulinate Synthase Variants Causes Protoporphyrin IX Accumulation and Light-Induced Mammalian Cell Death. *PLoS ONE* **2014**, *9*, e93078. [CrossRef]
56. Kaplan, E.L.; Meier, P. Nonparametric Estimation from Incomplete Observations. *J. Am. Stat. Assoc.* **1958**, *53*, 457–481. [CrossRef]
57. Mantel, N. Evaluation of survival data and two new rank order statistics arising in its consideration. *Cancer Chemother. Rep.* **1966**, *50*, 163–170.
58. Krieg, R.C.; Messmann, H.; Rauch, J.; Seeger, S.; Knuechel, R. Metabolic characterization of tumor cell-specific protoporphyrin IX accumulation after exposure to 5-aminolevulinic acid in human colonic cells. *Photochem. Photobiol.* **2002**, *76*, 518–525. [CrossRef]
59. Díaz, M.I.; Díaz, P.; Bennett, J.C.; Urra, H.; Ortiz, R.; Orellana, P.C.; Hetz, C.; Quest, A.F.G. Caveolin-1 suppresses tumor formation through the inhibition of the unfolded protein response. *Cell Death Dis.* **2020**, *11*, 648. [CrossRef]
60. Martin, B.; Paesmans, M.; Mascaux, C.; Berghmans, T.; Lothaire, P.; Meert, A.P.; Lafitte, J.J.; Sculier, J.P. Ki-67 expression and patients survival in lung cancer: Systematic review of the literature with meta-analysis. *Br. J. Cancer* **2004**, *91*, 2018–2025. [CrossRef]

61. Lemech, C.R.; Kichenadasse, G.; Marschner, J.-P.; Alevizopoulos, K.; Otterlei, M.; Millward, M. ATX-101, a cell-penetrating protein targeting PCNA, can be safely administered as intravenous infusion in patients and shows clinical activity in a Phase 1 study. *Oncogene* **2023**, *42*, 541–544. [CrossRef]
62. Zhang, J.; Cheltsov, A.V.; Ferreira, G.C. Conversion of 5-aminolevulinate synthase into a more active enzyme by linking the two subunits: Spectroscopic and kinetic properties. *Protein Sci.* **2005**, *14*, 1190–1200. [CrossRef]
63. Shi, Z.; Ferreira, G.C. A continuous anaerobic fluorimetric assay for ferrochelatase by monitoring porphyrin disappearance. *Anal. Biochem.* **2003**, *318*, 18–24. [CrossRef]
64. Koukourakis, M.I.; Kalamida, D.; Mitrakas, A.G.; Liousia, M.; Pouliliou, S.; Sivridis, E.; Giatromanolaki, A. Metabolic cooperation between co-cultured lung cancer cells and lung fibroblasts. *Lab. Investig.* **2017**, *97*, 1321–1331. [CrossRef]
65. Zilionis, R.; Engblom, C.; Pfirschke, C.; Savova, V.; Zemmour, D.; Saatcioglu, H.D.; Krishnan, I.; Maroni, G.; Meyerovitz, C.V.; Kerwin, C.M.; et al. Single-Cell Transcriptomics of Human and Mouse Lung Cancers Reveals Conserved Myeloid Populations across Individuals and Species. *Immunity* **2019**, *50*, 1317–1334.e1310. [CrossRef]
66. Bhattacharya, S.; Prajapati, B.G.; Singh, S.; Anjum, M.M. Nanoparticles drug delivery for 5-aminolevulinic acid (5-ALA) in photodynamic therapy (PDT) for multiple cancer treatment: A critical review on biosynthesis, detection, and therapeutic applications. *J. Cancer Res. Clin. Oncol.* **2023**, *149*, 17607–17634. [CrossRef]
67. Casas, A. Clinical uses of 5-aminolaevulinic acid in photodynamic treatment and photodetection of cancer: A review. *Cancer Lett.* **2020**, *490*, 165–173. [CrossRef]
68. Ebrahimi, S.; Khaleghi Ghadiri, M.; Stummer, W.; Gorji, A. Enhancing 5-ALA-PDT efficacy against resistant tumor cells: Strategies and advances. *Life Sci.* **2024**, *351*, 122808. [CrossRef]
69. Marcus, S.L.; Sobel, R.S.; Golub, A.L.; Carroll, R.L.; Lundahl, S.; Shulman, D.G. Photodynamic therapy (PDT) and photodiagnosis (PD) using endogenous photosensitization induced by 5-aminolevulinic acid (ALA): Current clinical and development status. *J. Clin. Laser Med. Surg.* **1996**, *14*, 59–66. [CrossRef]
70. Shinoda, Y.; Kato, D.; Ando, R.; Endo, H.; Takahashi, T.; Tsuneoka, Y.; Fujiwara, Y. Systematic Review and Meta-Analysis of In Vitro Anti-Human Cancer Experiments Investigating the Use of 5-Aminolevulinic Acid (5-ALA) for Photodynamic Therapy. *Pharmaceuticals* **2021**, *14*, 229. [CrossRef]
71. Vicente, M.G. Porphyrin-based sensitizers in the detection and treatment of cancer: Recent progress. *Curr. Med. Chem. Anticancer Agents* **2001**, *1*, 175–194. [CrossRef]
72. Allison, R.; Moghissi, K.; Downie, G.; Dixon, K. Photodynamic therapy (PDT) for lung cancer. *Photodiagnosis Photodyn. Ther.* **2011**, *8*, 231–239. [CrossRef]
73. Simone, C.B., 2nd; Cengel, K.A. Photodynamic therapy for lung cancer and malignant pleural mesothelioma. *Semin. Oncol.* **2014**, *41*, 820–830. [CrossRef]
74. Wang, K.; Yu, B.; Pathak, J.L. An update in clinical utilization of photodynamic therapy for lung cancer. *J. Cancer* **2021**, *12*, 1154–1160. [CrossRef]
75. Martínez-Reyes, I.; Chandel, N.S. Cancer metabolism: Looking forward. *Nat. Rev. Cancer* **2021**, *21*, 669–680. [CrossRef]
76. Marongiu, F.; Doratiotto, S.; Sini, M.; Serra, M.P.; Laconi, E. Cancer as a disease of tissue pattern formation. *Prog. Histochem. Cytochem.* **2012**, *47*, 175–207. [CrossRef]
77. de Visser, K.E.; Joyce, J.A. The evolving tumor microenvironment: From cancer initiation to metastatic outgrowth. *Cancer Cell* **2023**, *41*, 374–403. [CrossRef]
78. Kanzaki, R.; Pietras, K. Heterogeneity of cancer-associated fibroblasts: Opportunities for precision medicine. *Cancer Sci.* **2020**, *111*, 2708–2717. [CrossRef]
79. Dagogo-Jack, I.; Shaw, A.T. Tumour heterogeneity and resistance to cancer therapies. *Nat. Rev. Clin. Oncol.* **2018**, *15*, 81–94. [CrossRef]
80. Meacham, C.E.; Morrison, S.J. Tumour heterogeneity and cancer cell plasticity. *Nature* **2013**, *501*, 328–337. [CrossRef]
81. Shanmugam, M.; McBrayer, S.K.; Rosen, S.T. Targeting the Warburg effect in hematological malignancies: From PET to therapy. *Curr. Opin. Oncol.* **2009**, *21*, 531–536. [CrossRef]
82. Meng, Y.; Sun, J.; Zhang, G.; Yu, T.; Piao, H. Imaging glucose metabolism to reveal tumor progression. *Front. Physiol.* **2023**, *14*, 1103354. [CrossRef]
83. Batra, S.; Adekola, K.U.; Rosen, S.T.; Shanmugam, M. Cancer metabolism as a therapeutic target. *Oncology* **2013**, *27*, 460–467.
84. Namikawa, T.; Yatabe, T.; Inoue, K.; Shuin, T.; Hanazaki, K. Clinical applications of 5-aminolevulinic acid-mediated fluorescence for gastric cancer. *World J. Gastroenterol.* **2015**, *21*, 8769–8775. [CrossRef]
85. Mahmoudi, K.; Garvey, K.L.; Bouras, A.; Cramer, G.; Stepp, H.; Jesu Raj, J.G.; Bozec, D.; Busch, T.M.; Hadjipanayis, C.G. 5-aminolevulinic acid photodynamic therapy for the treatment of high-grade gliomas. *J. Neurooncol.* **2019**, *141*, 595–607. [CrossRef]
86. Yu, H. Depolarization or hyperpolarization: Emerging role of altered bioelectricity in breast cancer metastasis. *EBioMedicine* **2022**, *76*, 103853. [CrossRef]
87. Quicke, P.; Sun, Y.; Arias-Garcia, M.; Beykou, M.; Acker, C.D.; Djamgoz, M.B.A.; Bakal, C.; Foust, A.J. Voltage imaging reveals the dynamic electrical signatures of human breast cancer cells. *Commun. Biol.* **2022**, *5*, 1178. [CrossRef]
88. Carvalho, J. A bioelectric model of carcinogenesis, including propagation of cell membrane depolarization and reversal therapies. *Sci. Rep.* **2021**, *11*, 13607. [CrossRef]

89. Pignatelli, P.; Umme, S.; D'Antonio, D.L.; Piattelli, A.; Curia, M.C. Reactive Oxygen Species Produced by 5-Aminolevulinic Acid Photodynamic Therapy in the Treatment of Cancer. *Int. J. Mol. Sci.* **2023**, *24*, 8964. [CrossRef]
90. Zhang, L.; Zhu, B.; Zeng, Y.; Shen, H.; Zhang, J.; Wang, X. Clinical lipidomics in understanding of lung cancer: Opportunity and challenge. *Cancer Lett.* **2020**, *470*, 75–83. [CrossRef]
91. Sayin, V.I.; LeBoeuf, S.E.; Papagiannakopoulos, T. Targeting Metabolic Bottlenecks in Lung Cancer. *Trends Cancer* **2019**, *5*, 457–459. [CrossRef] [PubMed]